



JGR Space Physics

RESEARCH ARTICLE

10.1029/2022JA030980

Key Points:

- Earthward moving ion particles originating near the magnetotail reconnection region are traced self-consistently in a global hybrid simulation
- The most intense acceleration in a short period is due to particles' encounter with a fast-flow electric field
- A great portion of the energetic particles is found to transport to the inner magnetosphere

Correspondence to:

Z. Guo and F. Shi, guozf@cugb.edu.cn; fzs0002@auburn.edu

Citation:

Shi, F., Guo, Z., Lin, Y., Wang, X., & Cheng, L. (2023). Magnetotail ion acceleration in 3-D global hybrid simulations. *Journal of Geophysical Research: Space Physics*, 128, e2022JA030980. https://doi.org/10.1029/2022JA030980

Received 2 SEP 2022 Accepted 20 APR 2023

Author Contributions:

Conceptualization: Zhifang Guo

Data curation: Zhifang Guo
Formal analysis: Zhifang Guo
Funding acquisition: Yu Lin
Methodology: Lei Cheng
Project Administration: Yu Lin
Software: Xueyi Wang
Supervision: Yu Lin
Validation: Zhifang Guo
Visualization: Zhifang Guo
Writing – original draft: Feng Shi
Writing – review & editing: Feng Shi,
Zhifang Guo, Yu Lin, Lei Cheng

© 2023. American Geophysical Union. All Rights Reserved.

Magnetotail Ion Acceleration in 3-D Global Hybrid Simulations

Feng Shi¹ D, Zhifang Guo^{1,2} D, Yu Lin¹ D, Xueyi Wang¹ D, and Lei Cheng³ D

¹Department of Physics, Auburn University, Auburn, AL, USA, ²School of Geophysics and Information Technology, China University of Geosciences, Beijing, China, ³Department of Aerospace, Physics and Space Sciences, Florida Institute of Technology, Melbourne, FL, USA

Abstract Particle injection by magnetotail reconnection plays an important role in the magnetospheric physics, since these particles may be accelerated to high energy and constituent energetic particles in the inner magnetosphere. In this paper, we trace such ion particles from a near-Earth reconnection region to the inner magnetosphere self-consistently in a 3-D global hybrid simulation using ANGIE3D, and demonstrate the important roles of the earthward fast flows in the ion acceleration process in the tail plasma sheet. Although the particles can gain several times of their initial energy from the reconnection X-line region, a dramatic increase of the ion energy (from a few keV up to a few tens of keV) occurs in a very short period of time due to their encounter with the earthward fast flows. A large portion (\$\times 70\%) of the earthward moving particles around the focused reconnection site encounter fast flows and are significantly accelerated. Our results indicate that fast flow electric fields play major roles, as opposed to other common mechanisms such as the adiabatic Betatron and Fermi processes, in ion acceleration from the near-tail region to the inner magnetosphere. In addition, dipolarization fronts associated with magnetic reconnection also affect the particle acceleration. On the global scale, it is found that particles can encounter the reconnection region first and then return to the fast flows multiple times, and thus the acceleration is through multiple local acceleration processes, leading to particle energy ~50 keV by reconnection/fast flows in the tail. The global simulation shows that particle acceleration involves multiple regions during their injection into the ring current.

1. Introduction

A major consequence of space plasma activities associated with magnetic reconfiguration is the generation of the suprathermal particles, which results in an increased flux of energetic particle fluxes (Kivelson & Russell, 1995; Parks et al., 1968; Yamada et al., 2007). One of the primary sites where magnetospheric particle acceleration is often observed lies in the magnetotail. Moreover, energetic particle events in the magnetotail are often observed in association with geomagnetic substorms (e.g., Arnoldy & Chan, 1969; Baker et al., 1981; Lezniak et al., 1968).

The most common mechanisms of particle acceleration in this context may be categorized into the following two classes: acceleration by magnetotail reconnection and acceleration during particle earthward transport. Previous numerous energetic particles have been observed around the reconnection region in the tail reconnection events (Chen et al., 2008; Hoshino et al., 2001; Imada et al., 2007; Øieroset et al., 2002; Retinò et al., 2008). Using two-dimensional (2-D) kinetic simulations, Pritchett (2006) and Ricci et al. (2003) found that electrons could be accelerated due to the existence of the electric field close to the reconnection X-line. Electron acceleration was also found due to the contraction (Drake & Shay, 2006; Wang et al., 2016) and the coalescence (Oka et al., 2010; Pritchett, 2008) of magnetic islands. Recent studies have observed that electrons can be directly accelerated by an electric field parallel to the magnetic field (E||) in the reconnection region (Egedal et al., 2012; Torbert et al., 2016), which have been found in 2-D particle-in-cell (PIC) simulations (Drake et al., 2003; Egedal et al., 2012). Drake et al. (2009) found that ions can be accelerated by the electric field around the magnetic separatrix region. Test particle simulations of M. Zhou et al. (2011) showed that ions can be accelerated by strong electric fields close to the X-line. Using 2-D PIC simulations, C. Z. Cheng et al. (2015) found both ions and electrons can be accelerated by the inductive electric field around the reconnection current layer and separatrix regions in the driven magnetic reconnection case with no guide field. Most of the aforementioned models are derived from the 2-D reconnection studies, while there is a substantial difference between three-dimensional (3-D) reconnection and 2-D reconnection (e.g., Daughton et al., 2011). The 3-D effects, such as the finite X-line lengths (1-5R_E, where R_E is the Earth radius) as obtained by Lin et al. (2014) and the dawn-dusk asymmetry

SHI ET AL.

of fast flows due to the presence of the Hall electric field (Lin et al., 2014; Lu et al., 2018, 2019; Lu, Lin, et al., 2016), are expected to significantly affect the ion acceleration process. So far, particle acceleration in 3-D dynamics is still poorly understood.

On the other hand, particles can subsequently be energized when they move out of the reconnection region and toward the Earth. It has been observed that the Betatron-type acceleration of electrons due to the compression of the magnetic field associated with dipolarization of magnetotail (Fu et al., 2011; Smets et al., 1999), along with the Fermi-type acceleration due to magnetic field line length contraction associated with the magnetic field collapse or dipolarization (e.g., Dahlin et al., 2016; Fu et al., 2011). Ashour-Abdalla et al. (1995) and Zelenyi et al. (2007) found that both ions and electrons can also gain energy through resonant orbit in the magnetotail. Previous studies have shown that the ions can be reflected and accelerated by the tail earthward propagating dipolarization fronts (DFs) (e.g., Eastwood et al., 2015; X. Zhou et al., 2010). On the global scale, the acceleration of magnetospheric ions from magnetotail into the inner magnetosphere is often observed related to the DFs (e.g., Ukhorskiy et al., 2017). Moreover, magnetospheric waves have been suggested to play an important role in the acceleration of both electrons and ions through wave-particle interactions (e.g., Fredricks, 1975; Gołkowski et al., 2019; Guo et al., 2017; Thorne et al., 2021).

In addition, it is suggested that part of the energy gained by ions in the magnetotail is carried along the magnetic field lines and dissipated by the ionosphere and upper layers of the ionized atmosphere (e.g., Lopez & Baker, 1994). It is also suggested that such energetic ions released from the substorm power the aurora displays, and thus affect ionospheric and ground current systems (Birn et al., 2012; Wing et al., 2007). The coupling between the distant magnetotail and the auroral dynamics is therefore one of the key aspects of understanding the global magnetospheric dynamics as well as its response to solar wind variability (Cowley & Lockwood, 1992; Kress et al., 2014; Milan et al., 2017).

Although in-situ spacecraft observations provide detailed information of such energetic charged particles, they often have to conjecture a global view of these accelerated particles as the whole process involves multiple plasma regions and/or boundary regions (e.g., Lyon, 2000). In this scenario, particle tracing calculations in 3-D global scale simulations play a key role in understanding the global picture (e.g., Birn et al., 1998, 2004). In addition, Eastwood et al. (2013) pointed out that modeling ion acceleration in such processes is crucial, since ions acquire most of the energy stored in the magnetic field by substorm reconnection, compared with electrons. In addition, since ions are not fully magnetized in most regions of the plasma sheet and can gain energy dramatically during their meandering movement, kinetic models are required in the study of the global scale accelerated ion motions from the reconnection sites toward the Earth (Runov et al., 2021).

3-D global magnetohydrodynamic (MHD) simulations coupled with test particle calculations have been used to study the enhanced ion precipitation in the magnetotail as well as the enhanced aurora phenomena (Birn et al., 1997, 2004; Pan et al., 2014; M. Zhou et al., 2011). Birn et al. (1997) found that ions can gain energy through a transverse electric field acceleration caused by the magnetic field dipolarization by tracing ion trajectories in the given electromagnetic fields from a 3-D MHD simulation, which is like the convection surge mechanism (Mauk, 1986; Quinn & Southwood, 1982). By tracing the ion orbits in a 3-D MHD simulation during a substorm event, M. Zhou et al. (2011) found particles were firstly accelerated by the electric fields close to the reconnection X-line, and subsequently accelerated by the electric field when they propagate toward the Earth from $x \sim -18R_{\rm F}$ to $x \sim -7R_{\rm F}$. Birn et al. (2012) examined the energetic ions injected into the inner magnetosphere by tracing test particles. They concluded that Betatron and Fermi accelerations associated with the dipolarization are the major ion acceleration mechanisms. The ion tracing study by Pan et al. (2014) found that ions first gained energy nonadiabatically near the reconnection site, and subsequently were adiabatically accelerated in the earthward propagating dipolarizations. The test particle approach, however, may not accurately account for the particle velocity-space information, for example, pitch-angle distribution, in their initial conditions. Moreover, since the plasma population is not negligible, the particles self-consistently interact with the electromagnetic field and can significantly affect the fields. How ions are energized in a global, kinetic system that contains the self-consistent particle-electromagnetic field interaction remains poorly understood.

In fully kinetic studies, on the other hand, although PIC models can cover both ion and electron scales, it is challenging to implement them on global-scale physics due to computational constraints (e.g., Eastwood et al., 2015). Hybrid models, in which ions are assumed to be individual particles while electrons are regarded as a fluid, do not resolve the electron-scale kinetic physics, so that the ion kinetic physics can be self-consistently simulated on

SHI ET AL. 2 of 16 global scales and dramatically reduce the computing expenses (e.g., Arzner & Scholer, 2001; Aunai et al., 2011; Lin et al., 2014).

In the present paper, we concentrate on the motions of ions that originate near the magnetotail reconnection region and investigate how they are accelerated in the self-consistent electromagnetic fields during their earthward orbits from the plasma sheet into the inner magnetosphere, by performing a 3-D global hybrid simulation using the ANGIE3D code (Lin et al., 2014, 2017). The focus of this study is on the near-tail region. Acceleration of ions from farther distances and going through multiple reconnection regions in the tail will not be addressed in this paper. The paper is structured as follows. In Section 2 we present the simulation model. Following that, simulation results are given in Section 3. Finally, conclusion and discussion are presented in Section 4.

2. Simulation Model

The 3-D global hybrid code ANGIE3D (Lin et al., 2014, 2017) is utilized to simulate the magnetotail reconnection and the associated ion particle dynamics, and the particle orbits are traced self-consistently. In the simulation, the ions are described as fully kinetic particles, while electrons are taken to be a massless fluid. We employ the Cartesian geocentric solar-magnetospheric coordinate system, in which the *x*-axis points from the Earth to the Sun and the *y*-axis is defined to be perpendicular to the Earth's magnetic dipole so that the x - z plane contains the dipole axis. The simulation domain covers $x \in [-60, +20]R_E$, $y \in [-30, +30]R_E$, and $z \in [-30, +30]R_E$, with the solar wind inflow boundary located at $x = 20R_E$. An electrostatic model of the magnetospheric-ionospheric coupling is applied for the inner boundary at $r = 3.5R_E$ (L. Cheng et al., 2020). More details of this hybrid model can be found elsewhere (L. Cheng et al., 2020; Lin et al., 2014).

In this paper, the interplanetary magnetic field B_0 is chosen as (0., 0., -10.) nT, corresponding to an ion gyrof-requency $\Omega_{i0} = 0.958 \, \mathrm{s}^{-1}$, the solar wind ion number density is $N_0 = 6 \, \mathrm{cm}^{-3}$, and the solar wind flows along the -x direction with a speed of 700 km/s. The solar wind ion inertial length is assumed as $d_{i0} = 0.1 \, \mathrm{R_E}$. The number of grid cells is $n_x \times n_y \times n_z = 337 \times 241 \times 217$, and a total of $\sim 2 \times 10^9$ particles are used. A smaller grid size of $\Delta x = \Delta y = \Delta z = 0.15 \, \mathrm{R_E}$ is used in the near-Earth region of $x \in [-25, 12] \, \mathrm{R_E}$, $y \in [-12, 12] \, \mathrm{R_E}$, and $z \in [-10, 10] \, \mathrm{R_E}$, while a larger grid size of $\sim 0.5 \, \mathrm{R_E}$ is set in $z > 10 \, \mathrm{R_E}$ outside the plasma sheet. The ion-scale kinetic physics with $\omega \sim \Omega_i$ and $k \rho_i \sim 1$ can be well resolved (Lin et al., 2014; Shi et al., 2021), where ω is the wave frequency, Ω_1 is local ion gryofrequency, k is the wave number, and ρ_i is the ion Larmor radius. Specifically, in our simulation, the ion inertial length in the tail is $d_i = d_{i0} \sqrt{N_0/N_i} \sim 0.2 \, \mathrm{R_E}$ based on a typical plasma sheet ion number density of $N_i \approx 0.3 \, N_0$. Therefore, the ion kinetic physics of $k \rho_i \sim 1$ in the hot plasma sheet of ion beta $\beta_i \sim 1$ or >1 can be well resolved with a spatial resolution of $0.15 \, \mathrm{R_E}$. To resolve the finite ion gyro-radius, we use a time step $\Delta t = 0.05 \, \Omega_{i0}^{-1}$, which is much smaller than the ion gyro-period (Lin et al., 2021). For the near-Earth dipole magnetic field region with strong field strengths, five sub-time steps are employed in the particle position advance to assure a higher time resolution. The global evolution, electromagnetic structure and waves associated with the tail reconnection of this case have been discussed by L. Cheng et al. (2020) and Lin et al. (2021).

In this study, we track the global scale ion acceleration from the near-Earth magnetotail reconnection region to the inner magnetosphere. The units used in the simulation results are presented as follows. The magnetic field B is in units of nT, the electric field is in V/m, time t is in seconds, the plasma flow velocities are in km/s, the particle energy is in keV, and the spatial length is in the Earth's radius R_E .

3. Simulation Results

3.1. Magnetotail Reconnection and Earthward Fast Flows

In our simulation, the bow shock, magnetopause, and magnetotail form self-consistently under the interaction between the constant southward IMF and the Earth's geomagnetic dipole field. The magnetotail is fully formed by $t \sim 2100$ s (L. Cheng et al., 2020). As described by Lin et al. (2014), dayside reconnection leads to a plasma sheet thinning in the growth phase as the magnetic flux propagates into the magnetotail lobes, followed by magnetotail reconnection in the thin current sheet. The tail reconnection is present between $x = -15R_{\rm E}$ and $-30R_{\rm E}$ with multiple X lines of $1 - 5R_{\rm E}$ lengths. The left and right plots of Figure 1 show the equatorial contours of magnetic field B and the x-component of the ion flow velocity V_{px} , respectively, in a global view at t = 2363 s (about 4 min after the magnetotail forms), with typical magnetic field lines also plotted in the plots. The Earth is located at

SHI ET AL. 3 of 16

wiley.com/doi/10.1029/2022JA030980 by Yu Lin

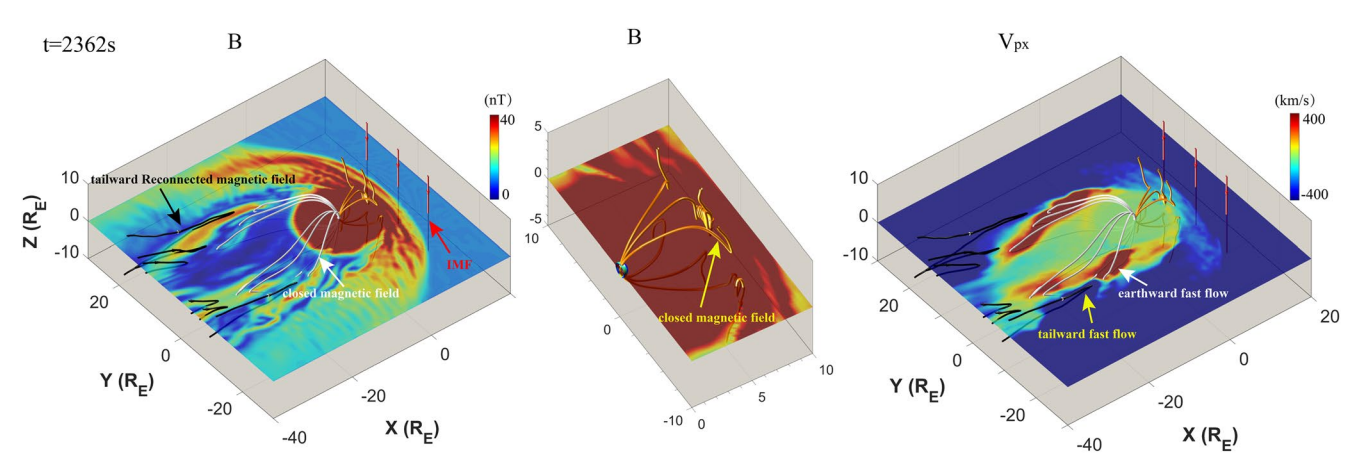


Figure 1. Equatorial magnetic field B (left) and ion flow velocity V_{px} (right) in the global view of near-Earth region at t = 2362 s. Typical magnetic field lines are also shown (red: unperturbed interplanetary magnetic field (IMF) lines; orange: reconnected field lines around the magnetopause; white: earthward reconnected/closed field lines in the tail; black: tailward reconnected field lines in the tail; green: stretched tail field lines with one end connecting to the Earth). The middle figure highlights reconnected field lines and flux ropes at the magnetopause under the southward IMF condition. Fast flows associated with the near-Earth reconnection on the dawn side are indicated.

the origin, and the distance from subsolar magnetopause and bow shock to the Earth can be seen at around 8R_E and $12R_{\rm F}$, respectively. The southward unperturbed IMF lines are shown by the red magnetic lines at $x \sim 15R_{\rm F}$ upstream of the quasi-perpendicular bow shock. On the nightside, the magnetic field lines colored in black and white depict the closed and reconnected magnetic field lines, respectively. In our simulations, reconnection is first triggered around $x \sim -20R_{\rm F}$ in the tail, followed by the presence of multiple reconnection sites. There are two near-tail reconnection regions, each on the dawn and dusk side. Relatively weak magnetic field strength is present in the reconnection regions. In the middle panel of Figure 1, the orange reconnected magnetic field lines as well as the magnetic flux ropes are clearly shown at the magnetopause around $x \sim 8R_F$, where the magnetic reconnection is intense under the southward IMF conditions (Guo et al., 2020). In the right panel of Figure 1, it can be seen that strong earthward plasma bulk flows generally coincide with the outflow region of the magnetotail reconnections, where reconnection sites can be determined by the X-type magnetic field line configuration, Hall-effect signatures of the ion diffusion region, as well as two opposite ion fast flows (Guo et al., 2020). There are two major earthward bursty bulk flows with speed of about 300-1000 km/s associated with two X lines in the near-tail region within $x \in [-25, -5]$ R_E. One X line is on the dawn side located around $(x, y, z) \sim (-16.2, -10.2, -10.2)$ 0) R_E with a length of $\sim 3R_E$. The other X line is on the dusk side, ranging from $(x, y, z) \sim (-30.1, 5.6, 0)R_E$ to $(x, y, z) \sim (-30.1, 5.6, 0)R_E$ $y, z > (-20.0, 11.6, 0)R_F$ oblique to the y direction. Such obliqueness is caused by the nonuniform and unsteady X-lines as well as the opposing magnetic tension forces acting on the dusk side and dawn side of the X-lines, which have been studied by Lu et al. (2015). Tailward of the dawn side X line, there exists another reconnection site around $x \sim -32R_{\rm F}$ but closer to midnight, which also generates an earthward fast flow but weaker than the fast flow of the dawn side X-line closer to the Earth.

3.2. Ion Acceleration

We focus on the acceleration processes of ions that originate around the near-Earth reconnection site of $y \sim [-10., -8]R_E$ (see Figure 1, and L. Cheng et al., 2020; Lin et al., 2021), which is on the dawn side, during their earthward orbits from the tail into the inner magnetosphere. This reconnection region of interest is located at $x \sim -16R_E$ at t = 2362 s, as described above. To understand the ion particle dynamics as a consequence of this near-tail reconnection, we trace particles originating from the vicinity of the reconnection region, within $x \in [-18, -14]R_E$, $y \in [-10, -8]R_E$, $z \in [0,1]R_E$ from t = 2362 s. Figure 2 shows the positions of traced particles in the simulation at t = 2362 s and t = 2505 s, respectively. The background contours show the flow velocity along the x-direction in the simulation. The total number of traced particles is 3804. A large portion of the traced particles moves toward the Earth in the simulation and have been accelerated significantly at t = 2505 s (see the energy of ions in the left panel), while some move tailward or go out of the simulation domain. In this paper, we are interested in the former particles that move into the inner magnetosphere and are accelerated as a consequence of magnetic reconnection.

SHI ET AL. 4 of 16

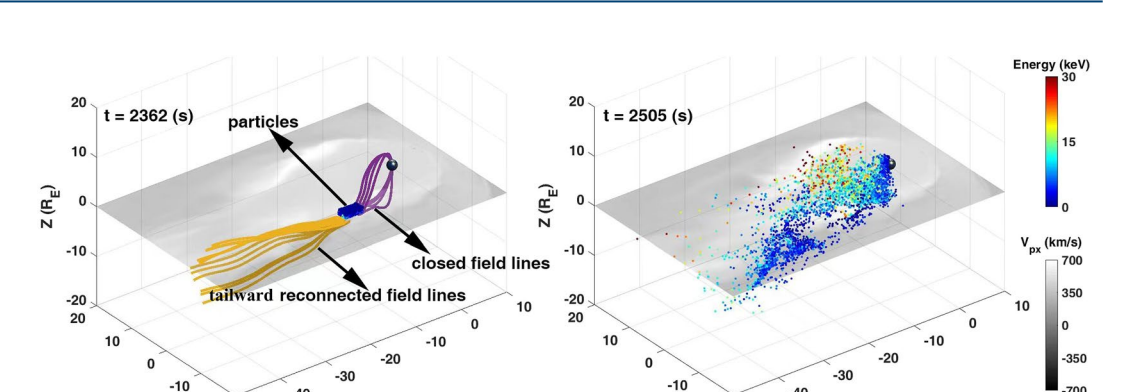


Figure 2. Positions of the traced particles (colored dots) in the simulation from t = 2362 s (left panel, with typical magnetic field lines) to t = 2505 s (right panel), respectively. The particles are colored by their energies in keV. The background contours show the x-component of the ion flow velocity. Initially (at t = 2362 s), low-energy particles are located near the reconnection site, and later at t = 2505 s a large portion of the particles have moved toward the Earth and accelerated significantly.

In our simulation, when the traced particles reach or pass through a sphere with a radius of $r=12\rm R_E$, we count the ions as the earthward moving particles. Our statistical counts show that a great portion (>60%–70%) of traced particles can move toward the Earth. Among these particles, when their speeds have a significant increase while they encounter the fast earthward flow, we record their acceleration as being related to the fast flow. It is found that about >90% of the earthward moving ions gain energy by encountering the fast flows. This portion of our traced particles can be seen in Figure 3, which shows the "velocity distribution" ($v_x - v_y$ and $v_x - v_z$) of the traced particles sampled within the initial regions of $x \in [-18, -14]\rm R_E$, $y \in [-10, -8]\rm R_E$, $z \in [0, 1]\rm R_E$ at t=2362 s (top) and then transport earthward to broader regions globally t=2505 s (bottom). Note that these distributions are not the velocity distributions at certain positions. At t=2362 s, all the traced particles are near the reconnection region (shown in Figure 2 left) with low energy (v_x , v_y , v_z are all near the origin in the velocity space). At a later time, t=2505 s, most of the particles are accelerated to ~ 1000 km/s, which is in the range of the fast flow speed. This result indicates that most of the earthward moving particles (>90%) are accelerated in association with the fast flows. The ring-shaped velocity distribution is formed as the earthward moving particles are trapped by the Earth's dipole field, bouncing between the northern and southern hemispheres.

Figure 4 shows the trajectories of 5 typical ion particles that originate from the reconnection site and then accelerate earthward. Note that the trajectories are color-coded by their energies so that their acceleration can be seen along the paths. The black and white flow contours clearly show the fast flows in opposite directions in the equatorial plane at the location where the traced particles initially reside. The initial tracing time is at the moment t = 2362 s. Around this moment, the traced particles enter the reconnection region and are accelerated by reconnection. It is seen that some particles move earthward, while others move tailward first and then move earthward. As seen from the flow contours, these particles are accelerated when they approach the dawn side fast flow region. These particles finally bounce between high latitude regions of north and south along the closed geomagnetic field lines.

To quantitatively show the resulting net acceleration after the particles are trapped by the Earth's dipole field as "ring current" particles, Figure 5 depicts the time variation of energy of these five particles. It is seen that the average energy of these particles is increased from ~ 2 to ~ 35 keV by the fast flow acceleration. The average energy of these particles when they are in the "ring current" (roughly shown in the shaded duration in Figure 5) is ~ 19.6 keV, which is much higher than their initial energy. These traced particles indeed gain significant energy from the earthward fast flows, and many then lose some energy (without considering other acceleration mechanisms in the inner magnetosphere) after they are trapped in the "ring current" region. Note that Particle 1 will be further analyzed in detail in this paper.

In order to gain more information of the particle acceleration by reconnection and fast flows, respectively, we choose the particle labeled as #1 in Figure 4 for detailed analysis. This particle moves tailward first and then earthward and through the fast flow region, and its two accelerations can be distinguished. Figure 6 shows various quantities along the chosen particle trajectory, including its energy, parallel velocity v_{\parallel} , x-component of the fast

SHI ET AL. 5 of 16

21699402, 2023, 5, Downloaded from https://agupubs.onlinelibrary.wiley.com/doi/10.1029/2022/A030980 by Yu Lin - Auburn University Libraries , Wiley Online Library on [06/05/2023]. See the Terms

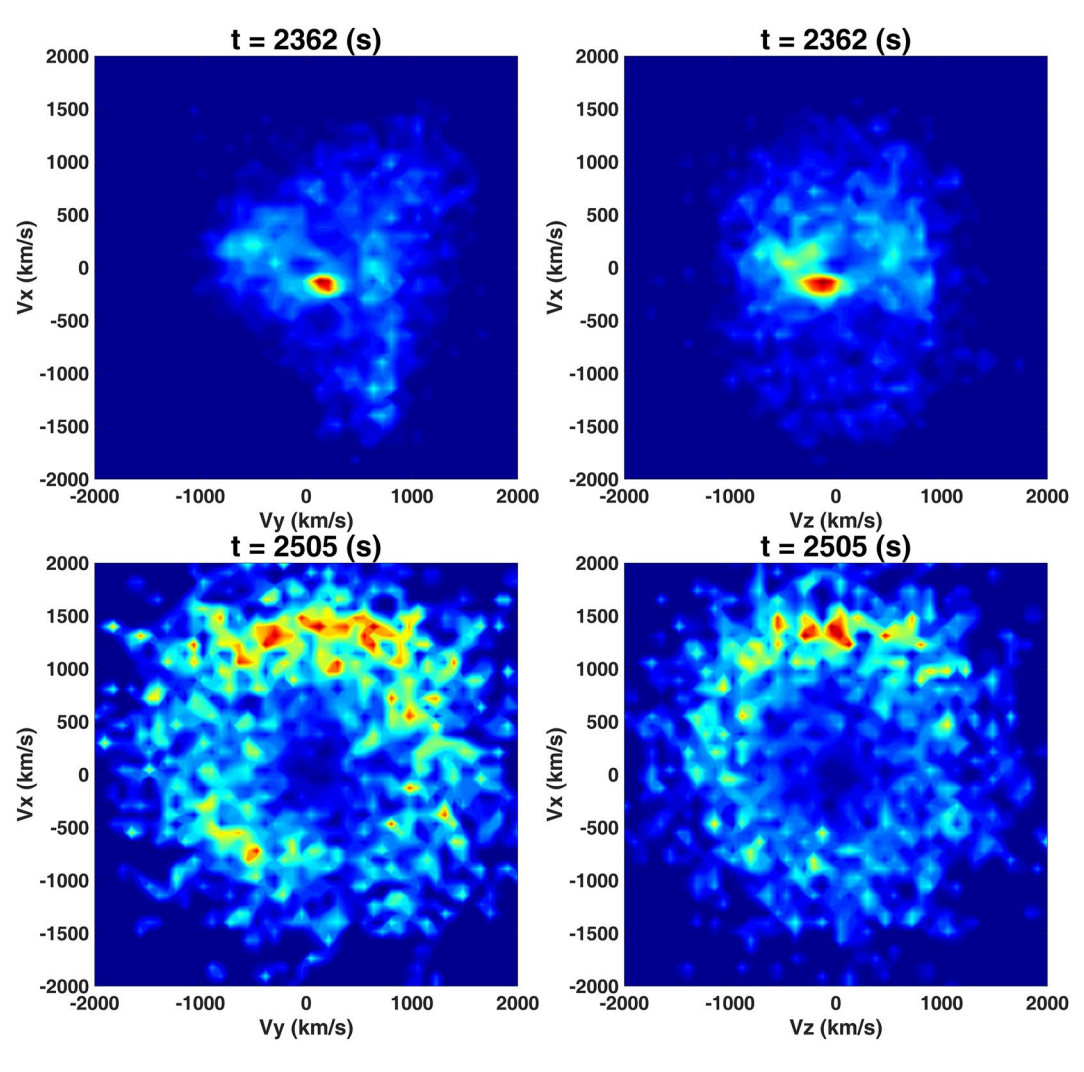


Figure 3. Velocity distributions $(v_x - v_y \text{ and } v_x - v_z)$ of traced particles at t = 2362 s (top) and t = 2505 s (bottom). Initially, the particles reside around the X-line region (shown in Figure 2, left) and of low energy. Later, most of the earthward moving particles (>90%) are accelerated to ~1000 km/s, which is consistent with the earthward fast flow speed. The ring-shaped distribution is formed because most of the earthward moving particles are trapped by the Earth's dipole field, bouncing and drifting as "ring current" particles.

flow V_{nv} , as well as the components of the magnetic field B, electric field E, particle position x, and its velocity v. The particle gyro-motion can be seen from the high-frequency oscillations of particle velocity. The yellow-shaded region marks the period when the particle is first accelerated by reconnection, and the initial acceleration is tailward from $(x, y, z) = (-16.2, -9.9, 0)R_F$ to $(x, y, z) = (-21.4, -7.6, 0.1)R_F$ along the oblique reconnection X-line at the dawn side (as shown in Figure 1) in the plasma sheet at $t \sim 2362-2400$ s. During $t \sim 2400-2420$ s, the particle moves away from the reconnection region. It is trapped in the current sheet (shown in Figure 4 for particle 1) while being accelerated (seen in the yellow shaded duration in the top right plot of Figure 6) to ~8.8 keV. Such acceleration process is similar to the pickup acceleration by the electric field in reconnection (C. Z. Cheng et al., 2015; Drake et al., 2009). This particle, however, is highly unmagnetized. Its acceleration during this period is predominantly by Hall electric field E_{y} perturbation (See the negative E_{y} in Figure 6.) in the ion diffusion region on the tailward side of the X line, where the negative flow velocity V_{px} is small, while being oscillating around the current sheet and confined by the Hall E_z component (pointing toward the current sheet from either side of the equator). The particle speed is increased to nearly 1.6 times the local Alfven speed. As the particle moves out of the strong Hall E, region and is accelerated duskward due to the positive E, it sees an earthward flow region just duskward of the dawn side X line (and a positive E, perturbation) due to reconnection at a tailward location (as seen in Figure 1 but at a later time). Subsequently, the motion direction of the particle changes from tailward

SHI ET AL. 6 of 16

21699402, 2023, 5, Downloaded from https://agupubs.onlinelibrary.wiley.com/doi/10.1029/2021/A030980 by Yu Lin - Auburn University Libraries , Wiley Online Library on [06/05/2023]

Figure 4. The trajectories (color-coded by their energy) of 5 typical ion particles (marked by different colors and indices) that go through the reconnection region and then accelerate earthward. The background equatorial contour is the bulk flow velocity at t = 2532 s, and the fast flow acceleration region is also marked. Particles undergo a dramatic increase in energy when they go through the earthward fast flow region along their paths as shown by the energy scale. The starting and ending particle positions at t = 2362 s and t = 2863 s are marked, respectively. The color scales for the background flow velocity and the particle energies along their trajectory are given on the right.

 $(v_x \sim -1300 \, \text{km/s})$ to earthward $(v_x \sim 1300 \, \text{km/s})$ (as shown in v_x in Figure 6) at $t \sim 2392$ s. Although this earthward flow generated by the tail side X line is not very strong, with $V_{px} \sim 410$ km/s as seen from the bottom right plot in Figure 6, the particle velocity v_x increases toward the Earth, while v_y and v_z also increases. During the above process, the particle is accelerated from ~ 2.5 to ~ 14.9 keV.

In $t \sim 2420$ –2500 s, the particle moves northward and earthward from the tail plasma sheet to high latitude in the tail region form $(x, y, z) = (-20.8, -5.2, -0.6)R_E$ to $(x, y, z) = (-9.2, -5.0, 1.7)R_E$, and then is reflected by the magnetic mirror point at $(x, y, z) = (-9.2, -5.0, 1.7)R_E$ in the northern hemisphere. Around t = 2524 s, being closer to the Earth, the particle goes through the strong earthward fast flow region associated with the near-Earth reconnection on the dawn side, and is dramatically accelerated while still moving along the field lines southward. The second reconnection/fast flow encounter ($t \sim 2408$ s and $t \sim 2524$ s) is seen from the bottom right plot of V_{px} . This period marks a major acceleration process that leads to the strongest increase in energy as shown in the pink-shaded region in Figure 6. The simulation shows that it is mainly the increase of E_y in the fast flow region and an associated DF (to be shown in Figure 7), contribute to the increase of the particle energy. As a result, a dramatic change in v_y is seen in Figure 6 at $t \sim 2535$ s.

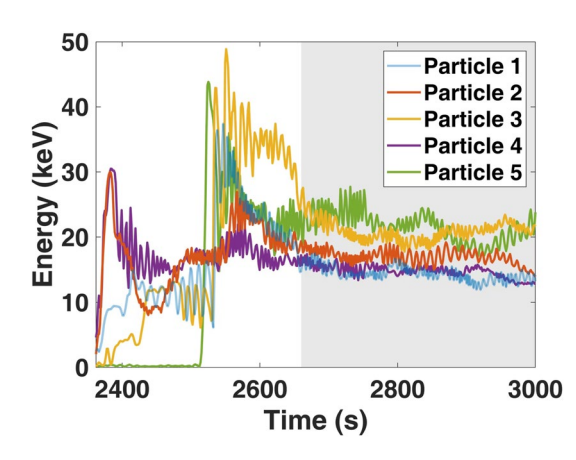


Figure 5. Energy of five typical earthward moving particles (traced in Figure 4) that go through the earthward fast flow region and are accelerated. The particles are accelerated dramatically by the earthward fast flow and then lose some energy after being trapped as "ring current" particles.

In the gray region in Figure 6 during t = 2550-2670 s, the particle energy gradually decreases, as also seen in Figure 5. The reason for the deceleration process is the following. While the particle being accelerated earthward by the fast flow electric field, it encounters the strong dipole-like magnetic field, as seen from the enhancement of all the field components B_{ν} , B_{ν} , and B_{σ} just after the pink-shaded duration in Figure 6. The positive plasma flow velocity V_{px} sharply decreases (not shown), whereas duskward bulk flow develops due to the ion duskward gradient and curvature drifts. The duskward flow $(V_{py} > 0)$ and the northward dipole field $(B_z > 0)$ lead to $E_x < 0$, as seen in the gray-shaded area in Figure 6. Meanwhile, $V_{px} > 0$ and the dipole-like field $B_v < 0$ on the dawn side lead to $E_z > 0$ (see also Figure 11). Particle 1 enters this region with gyro-averaged $v_x > 0$, $v_y > 0$, and $v_z < 0$ (moving southward and duskward in the dipole-like field). Although the particle duskward velocity and the dawn-dusk electric field ($E_{y} > 0$, significantly reduced outside the fast flow region) still lead to $E_v v_v > 0$, both $E_v v_r$ and $E_z v_z$ are negative, resulting in the deceleration of the particle. After the particle reaches its southmost position of $z \sim -4.87 R_{\rm F}$, it bounced northward in the dipole-like field until crossing the equator again around $t \sim 2596$ s. During this period, the particle velocity is reversed to $v_x < 0$ and $v_z > 0$. Although both $E_x v_x$ and $E_z v_z$ are

SHI ET AL. 7 of 16

21699402, 2023, 5, Downloaded from https://agupubs.onlinelibrary.wiley.com/doi/10.102920221A030980 by Yu Lin - Auburn University Libraries, Wiley Online Library on [06.052023]. See the Terms and Conditions (https://onlinelibrary.

conditions) on Wiley Online Library for rules of use; OA articles are governed by the applicable Creat

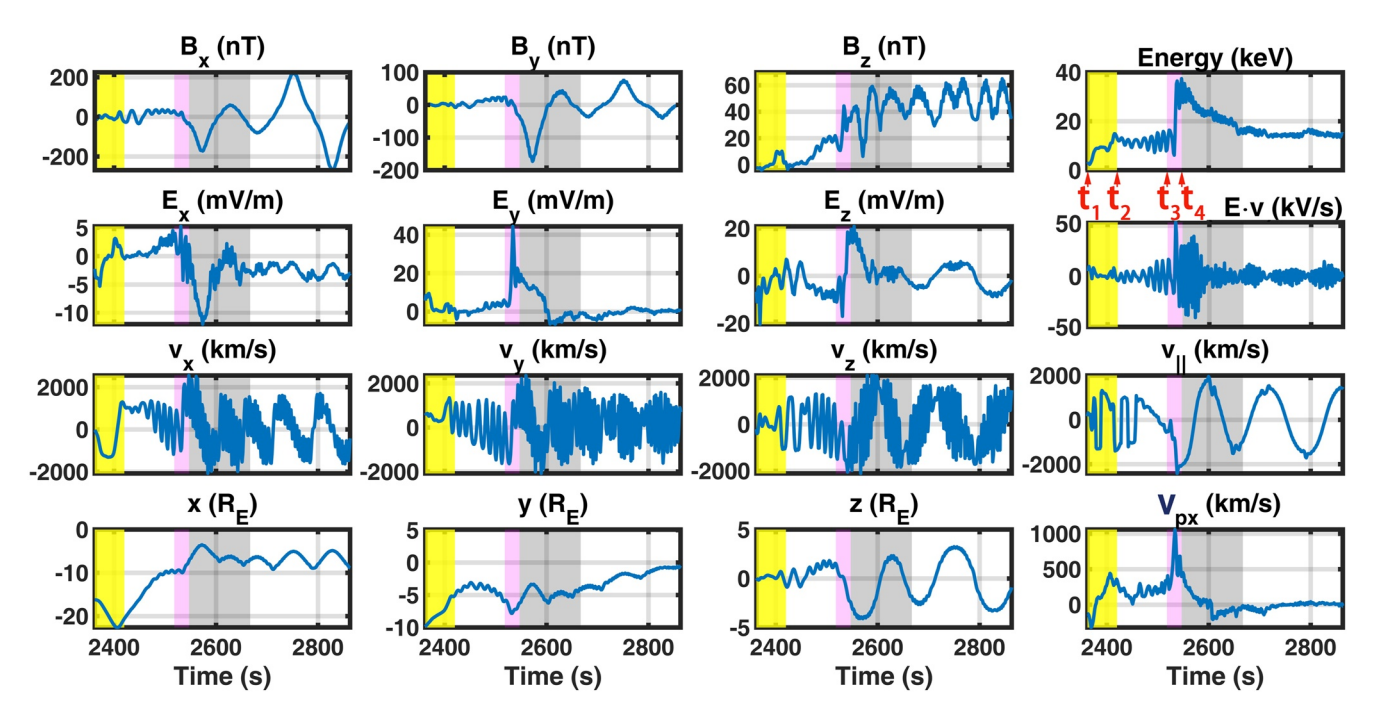


Figure 6. Various quantities along the trajectory of the traced particle #1. The yellow-shaded region shows the particle acceleration near the reconnection site, the pink region shows the particle's encounter with an earthward fast flow (outflow region of reconnection), and the gray region shows the particle deceleration in the inner magnetospheric region. Note that the time t_1 to t_4 shown in the top right panel of the energy plot corresponds to the starting initial time ($t_1 = 2362$ s), reconnection acceleration time ($t_2 = 2420$ s), fast flow encounter time ($t_3 = 2524$ s) and the moment after the fast flow acceleration ($t_4 = 2550$ s), respectively.

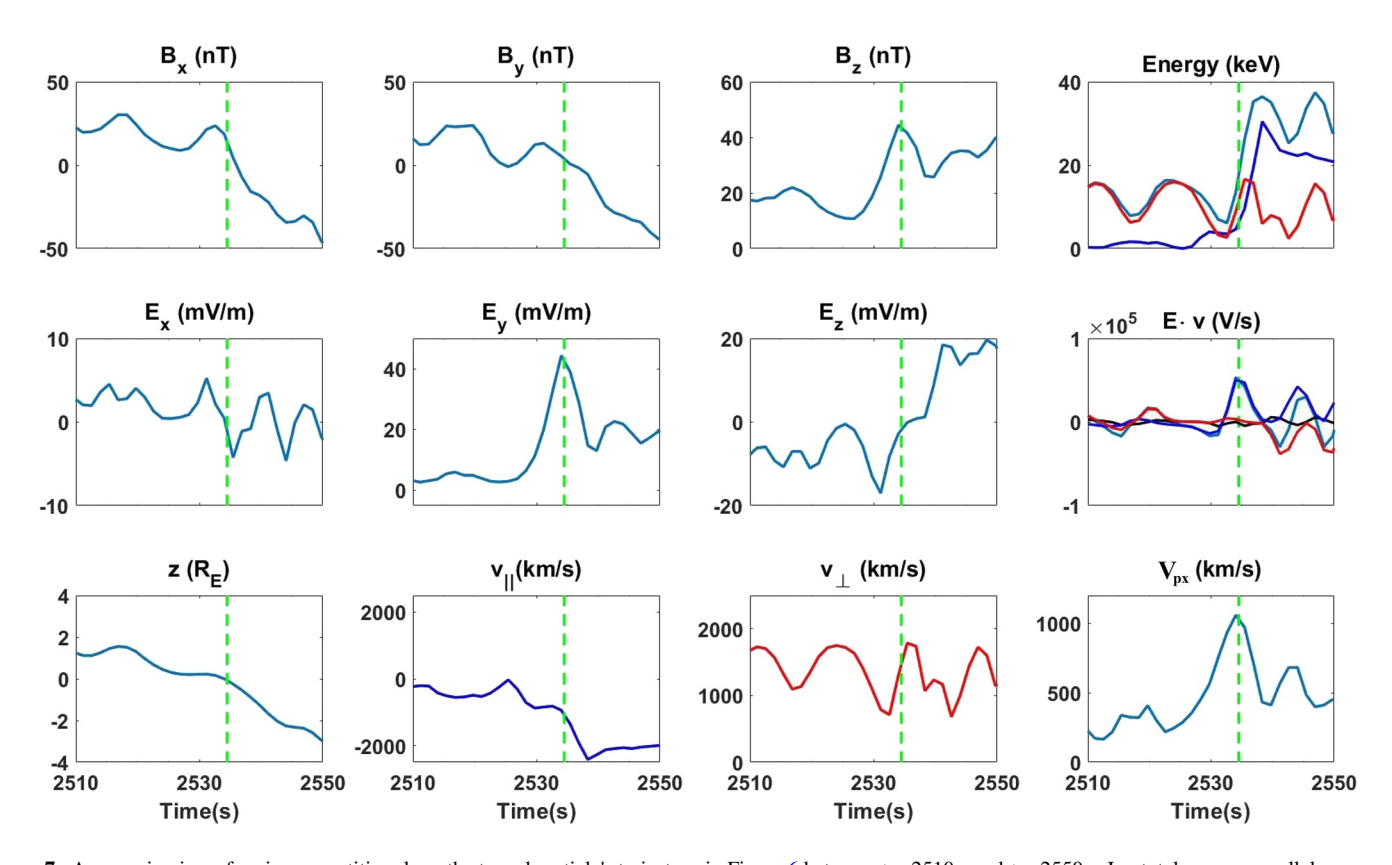


Figure 7. A zoom-in view of various quantities along the traced particle's trajectory in Figure 6 between t = 2510 s and t = 2550 s. Ion total energy, parallel energy, and perpendicular energy are shown as light blue line, blue line, and red line in the top right plot, respectively. The terms $E_x v_x$, $E_y v_y$ and $E_z v_z$ in the dot product $E \cdot v$ are plotted as black, blue, and red curves in the middle right plot.

SHI ET AL. 8 of 16

positive, E_z is significantly decreasing due to the diminishing bulk flow V_{px} . Meanwhile, the particle $v_y < 0$ leads to $E_y v_y < 0$. Overall, $E \cdot v < 0$, and the particle speed still decreases. Later, in t > 2652 s, both E_y and E_z are nearly zero, and a much gradual deceleration of the particle velocity is seen due to an overall $E_x v_x < 0$.

We now focus on the particle acceleration stage around fast flows. It can be seen that the particle energy is \sim 2.5, \sim 14.9, \sim 9.5, and \sim 36.5 keV at the starting time (t_1 = 2362 s), reconnection acceleration time (t_2 = 2420 s), fast flow encounter time (t_3 = 2524 s) and the moment after the fast flow acceleration (t_4 = 2550 s), respectively. Therefore, the particle energy increases \sim 6 times due to reconnection and \sim 15 times due to the earthward fast flow acceleration compared to the initial energy. For convenience, we will use t_1 , t_2 , t_3 and t_4 to refer these four moments in the following discussion.

To illustrate the detailed information of the particle acceleration associated with fast earthward flows and DF, Figure 7 depicts the zoom-in view of some quantities in Figure 6 between t = 2510 s and t = 2550 s, including the components of the magnetic field B, the particle energy (light blue line: total energy; blue line: parallel energy; red line: perpendicular energy), components of the electric field $E, E \cdot v$ (black line: $E_v v_v$; blue line: $E_v v_v$; red line: $E_z v_z$), particle position in z, its parallel velocity v_{\parallel} and perpendicular velocity v_{\perp} , and the x-component of the ion bulk flow V_{nx} . The fast flow reaches its maximum magnitude at t = 2536 s, as indicated by the vertical dashed green line. It can be seen that as the particle moves southward from the northern hemisphere, it encounters the fast earthward flow around the plasma sheet $(z \sim 0)$. In the meantime, it also runs into a DF where the B_z component sharply increases and the B_{ν} component slightly decreases. Due to the presence of the DF and fast earthward flow, the electric field E_y has a peak value of roughly 44.0 mV/m. The light blue line in the particle energy plot indicates that the particle is accelerated from 9.5 to 36.5 keV. The ion parallel energy (blue line) as well as its parallel velocity (v_{\parallel}) have both increased significantly. The ion perpendicular velocity gets only a little increase, indicating the Betatron acceleration mechanism plays very little role in this particle acceleration process. In addition, before the particles are trapped by the dipole field, there appears no obvious bounce motion, and thus the contribution of Fermi acceleration is also negligible. When the particle is accelerated by the fast flow and the DF, the quantity $E_{\nu}v_{\nu}$ is comparable with $E \cdot v$, indicating that the acceleration is dominated by E_{ν} , which is closely related to the fast flow and the DF. Therefore, the particle acceleration is aided by the electric field E_{ν} in the fast flow and DF. Compared to other common acceleration mechanisms, such as adiabatic Betatron and Fermi processes, our results show that the fast flow and DF associated with magnetic reconnection play a leading role in ion acceleration from the near-Earth magnetotail to the inner magnetosphere region. The spatial distribution of B_z , E_v and V_{nx} during the interaction between the particle and the fast flows/DF will be further examined in Figure 12.

As shown previously in Figure 6 yellow shaded region, the traced particle at t_1 is in the plasma sheet around z = 0. We take a detailed zoom-in view around this region in Figure 8 (top), which shows contour plots of the magnetic field strength B and the x-component flow velocity V_{px} in the x - y(z = 0) plane at time t_1 , respectively. Typical magnetic field lines are also shown in the figure. Note that the orange, green, and black lines denote open, reconnected, and closed magnetic field lines, respectively. The position of the traced particle at t_1 is marked by the pink dot at position $(x, y, z) = (-16.2, -9.9, 0)R_E$. It clearly shows that the particle is initially located in the X-line region of the magnetotail reconnection, while the earthward and tailward outflows can be distinguished from V_{px} .

Figure 8 (bottom) shows the contour plots of B and V_{px} at moment t_2 in the x-y plane at $z=-0.6R_E$. At moment t_2 , the traced particle has moved to the position $(x, y, z)=(-20.8, -5.2, -0.6)R_E$, shown by the smaller white star in Figure 8 (bottom). It can be seen that although the traced particle is still in the plasma sheet $(z \sim 0)$, it enters the outflow region of reconnection, and is accelerated from 2.5 to 14.9 keV. Note that the X-line is shown more clearly at moment t_1 in V_{px} in Figure 8 (top), where the opposite fast flows can be seen nearly along the particle path.

Figure 9 shows the magnitude of the magnetic field B and the three components of flow velocity V_p at $z = 0.5R_E$ when the traced particle starts to be accelerated by the earthward fast flows in the near-Earth at $t_3 = 2524$ s. From the magnetic field strength B, it is found that the particle at this moment is in the near Earth's region $(x, y, z) = (-10.1, -5.2, 0.5)R_E$. From the plasma flow velocity V_p , it is seen that the particle moves from the magnetotail in the earthward fast flows. As previously seen in Figure 4, the traced particle moves almost along the magnetic field lines from high latitude $(x, y, z) = (-9.2, -5.0, 1.7)R_E$ back to the equatorial region $(x, y, z) = (-10.1, -5.2, 0.5)R_E$ and encounters the earthward fast flows, which can be seen from the locally enhanced V_{py} and V_{pz} .

Structures of the electric field E and parallel ion temperature T_{\parallel} at $t_3 = 2524$ s can be seen in Figure 10. It is seen that E_v is locally enhanced compared with E_x and E_z , as previously mentioned in Figure 6. After the dramatic

SHI ET AL. 9 of 16

21699402, 2023, 5, Downloaded from https://agupubs.onlinelibrary.wiley.com/do/10.1029/2022/A030980 by Yu Lin - Auburn University Libraries , Wiley Online Library on [06/05/2023]. See the Terms

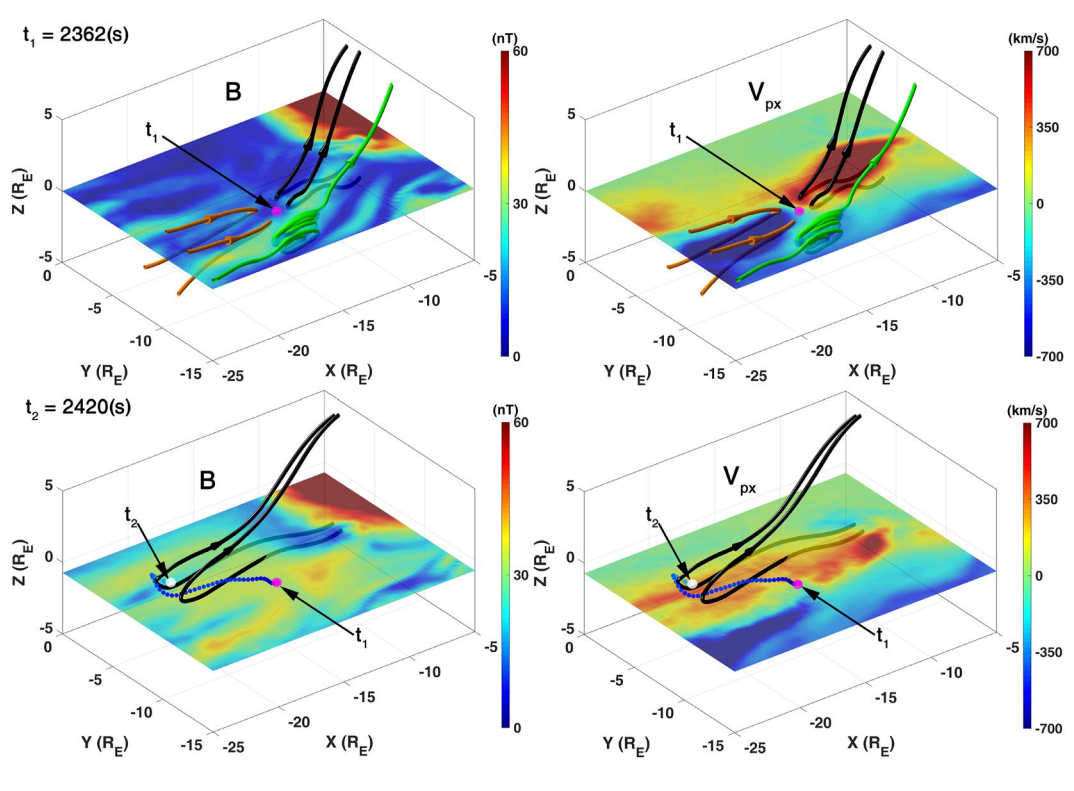


Figure 8. Contours of B and V_{px} in the x-y plane at z=0 at moment $t_1=2362$ s (top panel) and at $z=-0.6R_E$ at moment $t_2=2420$ s (bottom panel). Note that the x-y plane is placed at where the particle is at that instant. The pink dot marks the particle's position at moment t_1 , and the white dot marks the particle position at moments t_2 . The particle positions between t_1 and t_2 are also marked with the particle's trajectory shown by the blue dots. Orange, green, and black lines denote open, reconnected, and closed magnetic field lines, respectively.

acceleration, the particle moves further southward and earthward in the near-Earth dipole-like field region. From the temperature distribution T_{\parallel} at t_3 , it is seen that the plasma is locally heated.

At $t_4 = 2550$ s, the traced particle has been moved to $(x, y, z) = (-6.7, -6.1, -3.0)R_E$ and accelerated from 9.5 to 36.5 keV by the earthward fast flows, which is shown by the red dots along the particle trajectory near t_4 in Figure 11, with the position at t_4 also marked. Comparing V_{px} in Figures 9 and 11, it is seen that the earthward fast flows have slowed down, convecting bi-directionally to the dayside around $r = 10R_E$ in front of the strong dipole-like field. At this moment, the particle moves southward and duskward along the Earth's magnetic field line. The plasma flow velocity V, E_y, E_z and T_{\parallel} are also locally enhanced, as previously shown in Figure 6. After time t_4 , the particle moves out of this fast flow region, and thus it is not further accelerated but continues to move along the dipole field.

To get a clear view, we present a zoom-in view of B_z , E_y and V_{px} before (t = 2524 s) during (t = 2536 s) and after (t = 2550 s) the particle's encounter with the earthward fast flows as shown in Figure 12. The good correlation among B_z , E_y and V_{px} supports that the locally enhanced E_y is caused by the earthward fast flows. The black dots are the particle's positions at each moment, and the small colored dots represent the particle's trajectory and energy (the same energy scale as in Figure 4). The details of the particle acceleration processes associated with the earthward fast flow and the DF have been shown in Figures 6 and 7. Figures 12a-12c shows that the particle moves southward from the northern hemisphere at t = 2524 s. Later, at t = 2536 s, the particle reaches the plasma sheet and runs into the earthward fast flow and DF regions, where the electric field E_y has a peak value, as shown in Figures 12d-12f. It then undergoes a significant acceleration, resulting in a sharp increase in its energy, as shown by the colored dots in Figures 12g-12i. Subsequently, it moves out of the earthward fast flow and DF regions.

Overall, the above analysis of particle 1 shows that the fast flow electric field provides the most significant ion acceleration. Finally, we end this section by revisiting Figures 4 and 5 for the steps of acceleration of other four typical particles. Particle 3 is very similar to particle 1, first moving tailward from the reconnection site and getting its acceleration, then turning its trajectory earthward into the earthward fast flow and getting a second-stage major acceleration to \sim 49 keV. Particles 2 and 4, on the other hand, move earthward into the earthward outflow/fast

SHI ET AL. 10 of 16

21699402, 2023, 5, Downloaded from https://agupubs.onlinelibrary.wikey.com/doi/10.1029/2022J039980 by Yu Lin - Auburn University Libraries, Wikey Online Library on [06.052023]. See the Terms and Conditions (https://onlinelibrary.wikey.com/term

conditions) on Wiley Online Library for rules of use; OA articles are governed by the applicable Creative Commons

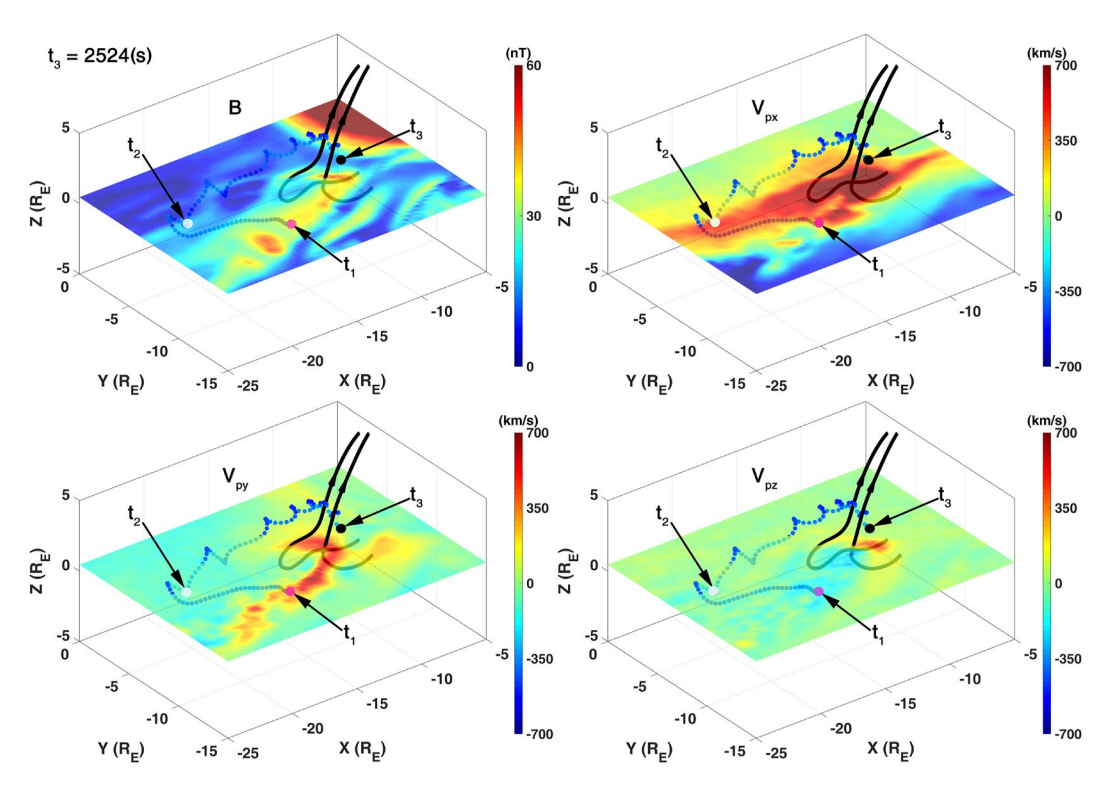


Figure 9. The traced particle's encounter of the earthward fast flows in the x - y ($z = 0.5 R_{\rm E}$) plane at moment $t_3 = 2524 {\rm s}$: B (top left), V_{px} (top right), V_{py} (bottom left), V_{pz} (bottom right). Typical magnetic field lines at t_3 and the particle trajectory are also shown. Note that the pink, white and dark dots mark the particle positions at moments t_1 , t_2 , and t_3 , respectively.

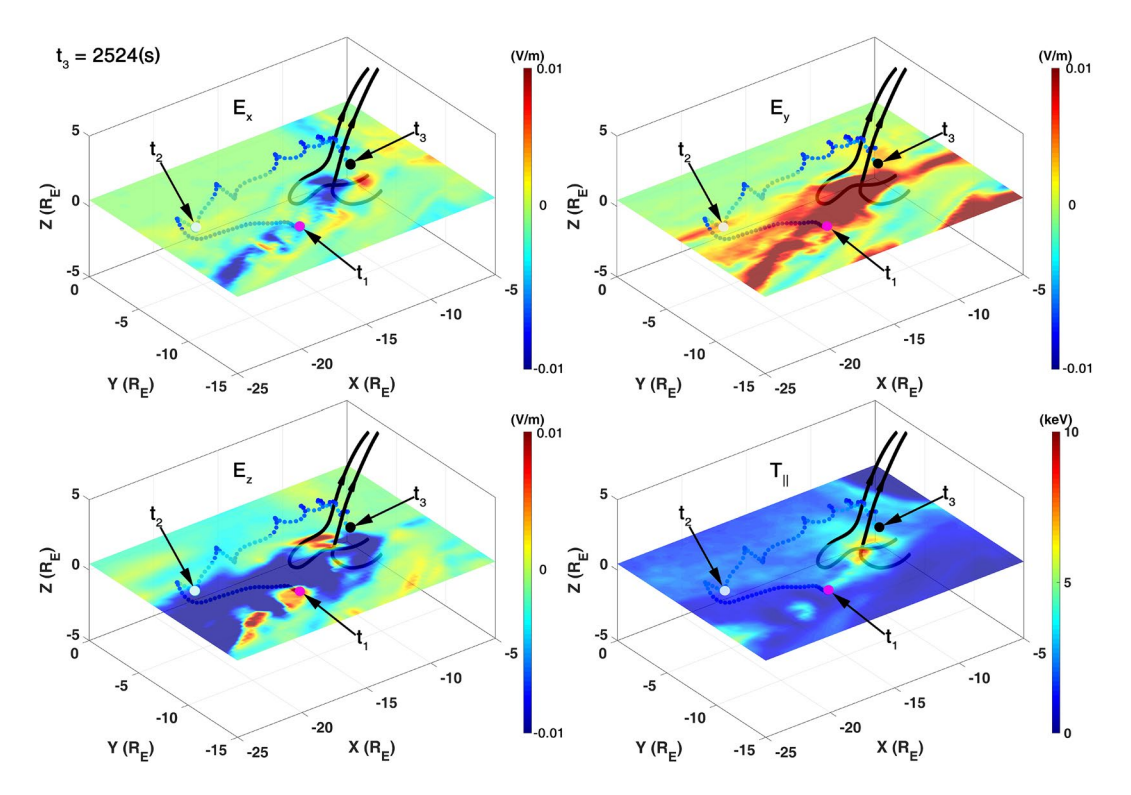


Figure 10. The traced particle's encounter of the earthward fast flows in the x - y (z = 0.5 R_E) plane at moment $t_3 = 2524$ s: E_x (top left), E_y (top right), E_z (bottom left), T_{\parallel} (bottom right). Typical magnetic field lines at t_3 and the particle trajectory are also shown. Note that the pink, white and dark dots mark the particle positions at moments t_1 , t_2 , and t_3 , respectively.

SHI ET AL. 11 of 16

21699402, 2023, 5, Downloaded from https://agupubs.onlinelibrary.wiley.com/doi/10.1029/2022JA030980 by Yu Lin - Auburn University Libraries, Wiley Online Library on [06/05/2023]. See the Terms and Conditions (https://onlinelibrary.

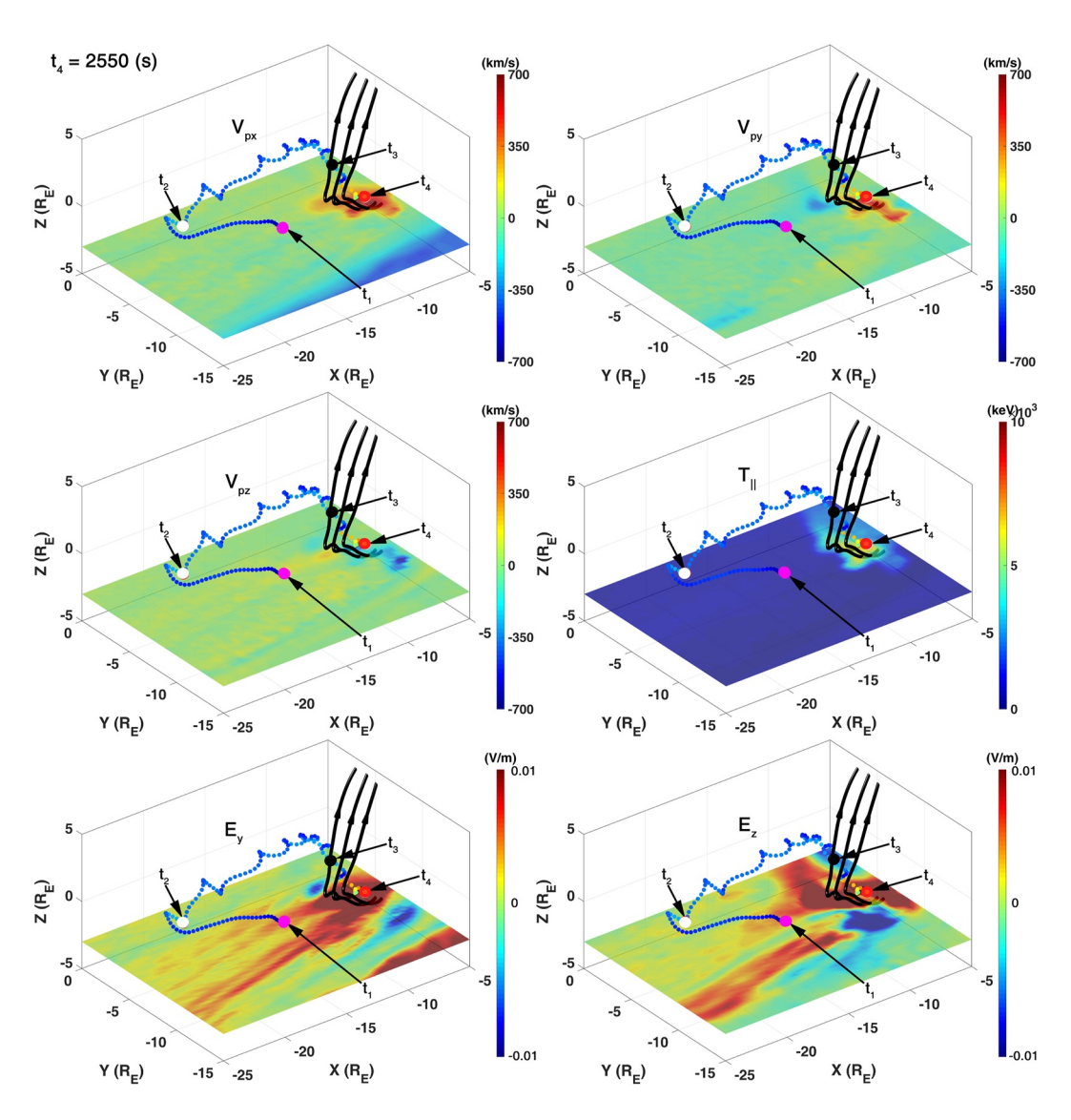


Figure 11. The traced particle position $(-6.7, -6.1, -3.0)R_E$ denoted by the red dot after its dramatic acceleration by the earthward fast flows near the Earth in the x-y ($z=-3.0R_E$) plane at moment $t_4=2550$ s. Contour plots at $z=-3.0R_E$ show V_{px} (top left), V_{py} (top right), V_{pz} (middle left), T_{\parallel} (middle right), E_y (bottom left), and E_z (bottom right) at t_4 . Typical magnetic field lines at time t_4 are also shown as black lines. The colored curve is the particle trajectory, same as in Figure 4. Note that the pink, white, black and red dots mark the particle positions at moments t_1 , t_2 , t_3 and t_4 , respectively, and they do not denote the particle energy at these moments.

flow region in the first place. They quickly gain dramatic accelerations. Particle 5 has a time delay before being picked up by electric field in reconnection (Drake et al., 2009). It then moves earthward in the reconnection layer and is significantly accelerated by the earthward fast flow electric field.

4. Conclusion and Discussion

In this paper, we have investigated ion particle acceleration from the near-Earth magnetotail reconnection region to the inner magnetosphere, by using a global hybrid simulation based on ANGIE3D. The main results are summarized as follows:

1. Ion particles from the reconnection site are accelerated by electric fields in reconnection (including the Hall electric field and the convection field), and a great portion $\gtrsim 60\%$ of ion particles can move toward the Earth. The traced particles can gain $\sim 4-5$ times of their energy near the reconnection site.

SHI ET AL. 12 of 16

onlinelibrary.wiley.com/doi/10.1029/2022JA030980 by Yu Lin - Auburn University Libraries , Wiley Online Library on [06/05/2023]. See the Terms

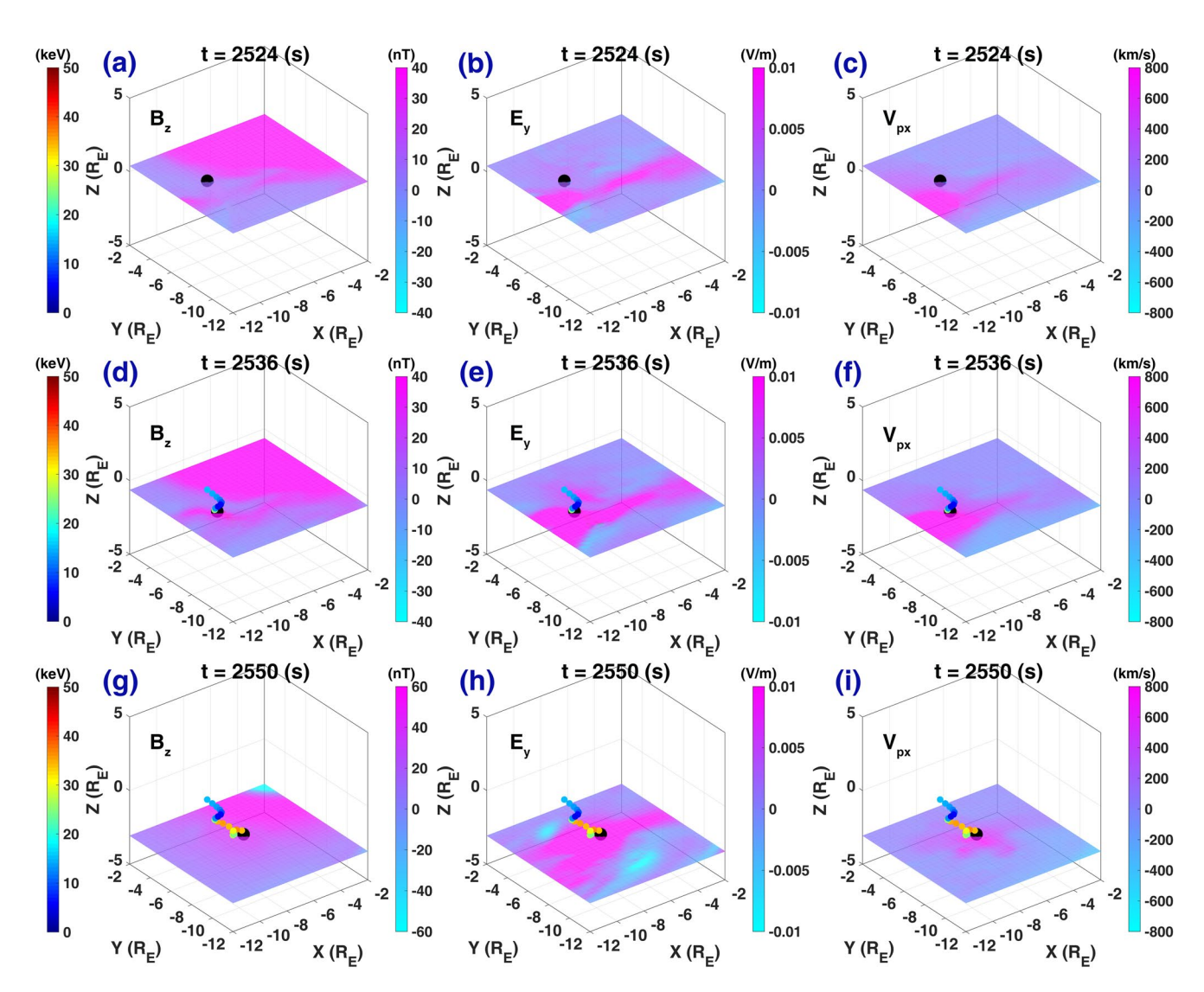


Figure 12. Acceleration of particle #1 before (a, b, and c), during (d, e, and f), and after (g, h, and i) the encounter of the earthward fast flows. The black dot represents the particle's position at each moment, and the colored dots show its positions from t = 2524-2550 s with the energy scale shown on the left. The components of B_z (a, d, and g), E_y (b, e, and h) and V_{nx} (c, f, and i) are also shown. Again the contour planes are shown at the particle's z positions at the corresponding instant.

- 2. More significant acceleration of ions takes place when they are in the fast flows.
- 3. When the traced particles move out of the reconnection/fast flow region, their acceleration is less significant, and they generally move along the magnetic field lines.
- 4. One typical particle trajectory moving toward the Earth is illustrated in detail. The particle gains energy in an initial phase by reconnection electric fields. Then, another dramatic increase of energy for the accelerated particle is found due to its encounter with the strong earthward fast flow. The acceleration by the fast flow electric field is observed much stronger (up to ~15 times of the initial energy) than the acceleration near the reconnection site. In the global process, particles may first be accelerated near the reconnection site and then encounter fast flows multiple times, being accelerated again. Our simulation also shows that about 70% of the particles originating near the reconnection site move toward the Earth and are accelerated by the earthward fast flows.
- 5. As particles continue move earthward after being accelerated by fast flows, they may lose a fraction of their peak energies in the fast flows while bouncing in the dipole-like field. Their net acceleration can be \sim 10 times.
- 6. Our simulation indicates that the particle acceleration is a global process, and its complete picture involves multiple regions of the magnetosphere.

Previous Geotail observations of Imada et al. (2015) studied the energetic ion acceleration during magnetic reconnection in the magnetotail. They found that most of the ions are locally accelerated to tens and even hundreds of

SHI ET AL. 13 of 16

keV downstream of reconnection outflow, which is associated with the fast flows. Based on 2-D PIC simulations, C. Z. Cheng et al. (2015) found that reconnection electric field provides the major ion acceleration mechanism. Also based on 2-D PIC simulations, Drake et al. (2009) showed that ion particles can be accelerated by the electric field, including both Hall electric fields and the convection electric field, in the reconnection exhausts without a guide field. A similar mechanism is found in our present global hybrid simulations for ion particle acceleration in the magnetotail, but the most significant energy enhancement is aided by the convection electric field in the fast flows. In 3-D, multiple reconnection regions of finite X-line lengths are present in the tail plasma sheet. On the global scale, particles can encounter the reconnection region first and then return to the fast flows multiple times at multiple locations, and thus the acceleration is through multiple local acceleration processes, leading to particle energy \sim 50 keV by reconnection/fast flows in the tail. Recent magnetospheric multiscale observations (e.g., Richard et al., 2022) have shown that magnetotail ions with gyroradii smaller than the spatial scale of the magnetic field structures are accelerated by the earthward fast flows, consistent with what we have seen for the acceleration of earthward moving ions in the simulation, although the spacecraft are located farther down the tail (< $-20R_E$) and the magnetic field in the observations is much smaller than what we have presented in the near-earth region (\le $-10R_E$).

In addition to the acceleration by fast flow electric field, Lu, Angelopoulos, et al. (2016) and X. Zhou et al. (2010) indicated that the charged particles can be accelerated when they are reflected by the approaching DF and moving ahead of it. Contribution of DF to ion acceleration has also been found in our simulation, although the DF does not appear to provide a major energy enhancement. The DF is found to result in a reflected ion beam in the velocity distribution in the near-tail region, as shown by Lin et al. (2021). Artemyev et al. (2012) suggested that when ion gyroradii become comparable with the scales of the magnetic field, ions can gain energy through the resonance acceleration. In our focused regions, however, we do not observe this large-scale resonance acceleration. As another possible source of acceleration, kinetic Alfven waves (KAWs) can be generated by near-tail reconnection, and then propagation earthward along field lines from the plasma sheet boundary layer (L. Cheng et al., 2020). Ion heating associated with KAWs has been shown in previous works of L. Cheng et al. (2020), Guo et al. (2016), and Liang et al. (2016). Regarding ion acceleration, however, our current particle tracing does not show a significant acceleration of ions by KAWs.

In this paper, we focus on the global-scale acceleration of earthward moving particles from the near-Earth magnetotail reconnection. In this region ($x < -16R_{\rm E}$) close to the Earth, magnetic flux ropes are less frequently formed, and the particle is not trapped by the flux rope from its trajectory. Although magnetic flux ropes generated at $x \sim -20R_{\rm E}$ can move earthward, its helicity can be released by the flow shear in the regions close to the Earth (L. Cheng et al., 2020). Our traced ions are from a specifically selected near-Earth region and cannot represent the entire magnetotail. Future studies are desirable to include the acceleration processes of ions originating from farther distances in the magnetotail, including those accelerated through multiple reconnection regions, with moving and/or interacting flux ropes and DFs.

Data Availability Statement

The numerical data used for generating the presented figures are available online (via https://doi.org/10.6084/m9.figshare.20522778.v5).

References

Arnoldy, R. L., & Chan, K. W. (1969). Particle substorms observed at the geostationary orbit. *Journal of Geophysical Research*, 74(21), 5019–5028. https://doi.org/10.1029/JA074i021p05019

Artemyev, A. V., Lutsenko, V. N., & Petrukovich, A. A. (2012). Ion resonance acceleration by dipolarization fronts: Analytic theory and spacecraft observation. *Annales Geophysicae*, 30(2), 317–324. https://doi.org/10.5194/angeo-30-317-2012

Arzner, K., & Scholer, M. (2001). Kinetic structure of the post plasmoid plasma sheet during magnetotail reconnection. *Journal of Geophysical Research*, 106(A3), 3827–3844. https://doi.org/10.1029/2000JA000179

Ashour-Abdalla, M., Zelenyi, L. M., Peroomian, V., Richard, R. L., & Bosqued, J. M. (1995). The mosaic structure of plasma bulk flows in the Earth's magnetotail. *Journal of Geophysical Research*, 100(A10), 19191–19209. https://doi.org/10.1029/95JA00902

Aunai, N., Belmont, G., & Smets, R. (2011). Proton acceleration in antiparallel collisionless magnetic reconnection: Kinetic mechanisms behind the fluid dynamics. *Journal of Geophysical Research*, 116(A9), A09232. https://doi.org/10.1029/2011JA016688

Baker, D. N., Belian, R. D., Higbie, P. R., Hones, E. W., Jr., & Stauning, P. (1981). Global properties of the magnetosphere during a substorm growth phase: A case study. *Journal of Geophysical Research*, 86(A11), 8941. https://doi.org/10.1029/JA086iA11p08941

Birn, J., Artemyev, A. V., Baker, D. N., Echim, M., Hoshino, M., & Zelenyi, L. M. (2012). Particle acceleration in the magnetotail and aurora. Space Science Reviews, 173(1–4), 49–102. https://doi.org/10.1007/s11214-012-9874-4

Acknowledgments

This work was supported by the National Science Foundation EPSCoR program fund (OIA-1655280) to Auburn University. Computer resources were provided by NASA Advanced Supercomputing (NAS) Division.

SHI ET AL. 14 of 16

- Birn, J., Thomsen, M. F., Borovsky, J. E., Reeves, G. D., Belian, D. J. M. R. D., & Hesse, M. (1997). Substorm ion injections: Geosynchronous observations and test particle orbits in three-dimensional dynamic MHD fields. *Journal of Geophysical Research*, 102(A2), 2325–2341. https://doi.org/10.1029/96JA03032
- Birn, J., Thomsen, M. F., Borovsky, J. E., Reeves, G. D., McComas, D. J., Belian, R. D., & Hesse, M. (1998). Substorm electron injections: Geosynchronous observations and test particle simulations. *Journal of Geophysical Research*, 103(A5), 9235–9248. https://doi.org/10.1029/97JA02635
- Birn, J., Thomsen, M. F., & Hesse, M. (2004). Electron acceleration in the dynamic magnetotail: Test particle orbits in three-dimensional MHD simulation fields. *Physics of Plasmas*, 11(5), 1825–1833. https://doi.org/10.1063/1.1704641
- Chen, L.-J., Bhattacharjee, A., Puhl-Quinn, P. A., Yang, H., Bessho, N., Imada, S., et al. (2008). Observation of energetic electrons within magnetic islands. *Nature Physics*, 4(1), 19–23. https://doi.org/10.1038/nphys777
- Cheng, C. Z., Inoue, S., Ono, Y., & Horiuchi, R. (2015). Physical processes of driven magnetic reconnection in collisionless plasmas: Zero guide field case. *Physics of Plasmas*, 22(10), 101205. https://doi.org/10.1063/1.4932337
- Cheng, L., Lin, Y., Perez, J. D., Johnson, J. R., & Wang, X. (2020). Kinetic Alfvén waves from magnetotail to the ionosphere in global hybrid simulation associated with fast flows. *Journal of Geophysical Research: Space Physics*, 125(2), e2019JA027062. https://doi. org/10.1029/2019JA027062
- Cowley, S. W., & Lockwood, M. (1992). Excitation and decay of solar-wind driven flows in the magnetosphere-ionosphere system. Annales Geophysicae, 10, 103–115.
- Dahlin, J. T., Drake, J. F., & Swisdak, M. (2016). Parallel electric fields are inefficient drivers of energetic electrons in magnetic reconnection. *Physics of Plasmas*, 23(12), 120704. https://doi.org/10.1063/1.4972082
- Daughton, W., Roytershteyn, V., Karimabadi, H., Yin, L., Albright, B. J., Bergen, B., & Bowers, K. J. (2011). Role of electron physics in the development of turbulent magnetic reconnection in collisionless plasmas. *Nature Physics*, 7(7), 539–542. https://doi.org/10.1038/nphys1965
- Drake, J. F., & Shay, M. A. (2006). The fundamentals of collisionless reconnection. In J. Birn & E. Priest (Eds.), *Reconnection of magnetic fields:*Magnetohydrodynamics and collisionless theory and observations. Cambridge University Press.
- Drake, J. F., Swisdak, M., Phan, T. D., Cassak, P. A., Shay, M. A., Lepri, S. T., et al. (2009). Ion heating resulting from pickup in magnetic reconnection exhausts. *Journal of Geophysical Research*, 114(A5), A05111. https://doi.org/10.1029/2008JA013701
- Drake, J. F., Swisdak, M., Shay, M. A., Rogers, B. N., Zeiler, A., & Cattell, C. (2003). Formation of electron holes and particle energization during magnetic reconnection. Science, 299(5608), 873–877. https://doi.org/10.1126/science.1080333
- Eastwood, J. P., Goldman, M. V., Hietala, H., Newman, D. L., Mistry, R., & Lapenta, G. (2015). Ion reflection and acceleration near magnetotail dipolarization fronts associated with magnetic reconnection. *Journal of Geophysical Research: Space Physics*, 120(1), 511–525. https://doi. org/10.1002/2014JA020516
- Eastwood, J. P., Phan, T. D., Drake, J. F., Shay, M. A., Borg, A. L., Lavraud, B., & Taylor, M. G. G. T. (2013). Energy partition in magnetic reconnection in Earth's magnetotail. *Physical Review Letters*, 110(22), 225001, https://doi.org/10.1103/PhysRevLett.110.225001
- Egedal, J., Daughton, W., & Le, A. (2012). Large-scale electron acceleration by parallel electric fields during magnetic reconnection. *Nature Physics*, 8(4), 321–324. https://doi.org/10.1038/nphys2249
- Fredricks, R. W. (1975). Wave-particle interactions in the outer magnetosphere: A review. *The Magnetospheres of the Earth and Jupiter*, 52, 113–152. https://doi.org/10.1007/978-94-010-1789-3_9
- Fu, H. S., Khotyaintsev, Y. V., André, M., & Vaivads, A. (2011). Fermi and betatron acceleration of suprathermal electrons behind dipolarization fronts. *Journal of Geophysical Research*, 38(16), L16104. https://doi.org/10.1029/2011GL048528
- Gołkowski, M., Harid, V., & Hosseini, P. (2019). Review of controlled excitation of non-linear wave-particle interactions in the magnetosphere. Frontiers in Astronomy and Space Sciences, 6, 2. https://doi.org/10.3389/fspas.2019.00002
- Guo, Z., Lin, Y., Wang, X., Vines, S. K., Lee, S. H., & Chen, Y. (2020). Magnetopause reconnection as influenced by the dipole tilt under south-ward IMF conditions: Hybrid simulation and MMS observation. *Journal of Geophysical Research: Space Physics*, 125(9), e2020JA027795. https://doi.org/10.1029/2020JA027795
- Guo, Z., Wu, M., & Du, A. (2016). Ion heating by Alfven waves associated with depolarization in the magnetotail: Two-dimensional global hybrid simulation. *Journal of Geophysical Research: Space Physics*, 121(2), 1124–1136. https://doi.org/10.1002/2015ja022068
- Guo, Z., Wu, M., & Du, A. (2017). Electron acceleration in the near-Earth magnetotail: Test particle calculations in electromagnetic fields from two-dimensional hybrid simulations. Astrophysics and Space Science, 362(7), 1–10. https://doi.org/10.1007/s10509-017-3093-0
- Hoshino, M., Mukai, T., Terasawa, T., & Shinohara, I. (2001). Suprathermal electron acceleration in magnetic reconnection. *Journal of Geophysics Research*, 106(A11), 25979–25978. https://doi.org/10.1029/2018JA025502
- Imada, S., Hirai, M., & Hoshino, M. (2015). Energetic ion acceleration during magnetic reconnection in the Earth's magnetotail. *Earth, Planets and Space*, 67(1), 203. https://doi.org/10.1186/s40623-015-0372-2
- Imada, S., Nakamura, R., Daly, P. W., Hoshino, M., Baumjohann, W., Muhlbachler, S., et al. (2007). Energetic electron acceleration in the down-stream reconnection outflow region. *Journal of Geophysical Research*, 112(A3), A03202. https://doi.org/10.1029/2006JA011847
- Kivelson, M., & Russell, C. (1995). Introduction to space physics. Cambridge University Press. ISBN: 9780521457149.
- Kress, B. T., Hudson, M. K., & Paral, J. (2014). Rebuilding of the Earth's outer electron belt during 8-10 October 2012. Geophysical Review Letters, 41(3), 749–754. https://doi.org/10.1002/2013GL058588
- Lezniak, T. W., Arnoldy, R. L., Parks, G. K., & Winckler, J. R. (1968). Measurement and intensity of energetic electrons at the equator at 6.6 Re. *Radio Science*, 3(7), 710–714. https://doi.org/10.1002/rds196837710
- Liang, J., Lin, Y., Johnson, J. R., Wang, X., & Wang, Z. X. (2016). Kinetic Alfven waves in three-dimensional magnetic reconnection. *Journal of Geophysical Research: Space Physics*, 121(7), 6526–6548. https://doi.org/10.1002/2016ja022505
- Lin, Y., Wang, X., Lu, S., Perez, J. P., & Lu, Q. (2014). Investigation of storm time magnetotail and ion injection using three-dimensional global hybrid simulation. *Journal of Geophysical Research: Space Physics*, 119(9), 7413–7432. https://doi.org/10.1002/2014JA020005
- Lin, Y., Wang, X. Y., Fok, M.-C., Buzulukova, N., Perez, J. D., Cheng, L., & Chen, L.-J. (2021). Magnetotail-inner magnetosphere transport associated with fast flows based on combined global-hybrid and CIMI simulation. *Journal of Geophysical Research: Space Physics*, 126(3), e2020JA028405. https://doi.org/10.1029/2020JA028405
- Lin, Y., Wing, S., Johnson, J. R., Wang, X. Y., Perez, J. D., & Cheng, L. (2017). Formation and transport of entropy structures in the magnetotail simulated with a 3-D global hybrid code. *Geophysical Research Letters*, 44(12), 5892–5899. https://doi.org/10.1002/2017GL073957
- Lopez, R., & Baker, D. (1994). Evidence for particle acceleration during magnetospheric substorms. International Astronomical Union Colloquium, 142, 531–539. https://doi.org/10.1017/S0252921100077770
- Lu, S., Angelopoulos, V., & Fu, H. (2016). Suprathermal particle energization in dipolarization fronts: Particle-in-cell simulations. *Journal of Geophysical Research: Space Physics*, 121(10), 9483–9500. https://doi.org/10.1002/2016ja022815

SHI ET AL. 15 of 16

- Lu, S., Artemyev, A. V., Angelopoulos, V., Lin, Y., Zhang, X.-J., Liu, J., et al. (2019). The Hall electric field in Earth's magnetotail thin current sheet. *Journal of Geophysical Research: Space Physics*, 124(2), 1052–1062. https://doi.org/10.1029/2018ja026202
- Lu, S., Lin, Y., Angelopoulos, V., Artemyev, A. V., Pritchett, P. L., Lu, Q., & Wang, X. Y. (2016). Hall effect control of magnetotail dawn-dusk asymmetry: A three-dimensional global hybrid simulation. *Journal of Geophysical Research: Space Physics*, 121(12), 11882–11895. https://doi.org/10.1002/2016JA023325
- Lu, S., Lin, Y., Lu, Q. M., Wang, X. Y., Wang, R. S., Huang, C., et al. (2015). Evolution of flux ropes in the magnetotail: A three-dimensional global hybrid simulation. *Physics of Plasmas*, 22(5), 052901. https://doi.org/10.1063/1.4919615
- Lu, S., Pritchett, P. L., Angelopoulos, V., & Artemyev, A. V. (2018). Formation of dawn-dusk asymmetry in Earth's magnetotail thin current sheet: A three-dimensional particle-in-cell simulation. *Journal of Geophysical Research: Space Physics*, 123(4), 2801–2814. https://doi. org/10.1002/2017ja025095
- Lyon, J. G. (2000). The solar wind-magnetosphere-ionosphere system. Science, 288(5473), 1987–1991. https://doi.org/10.1126/science.288.5473.1987
- Mauk, B. H. (1986). Quantitative modeling of the "convection surge" mechanism of ion acceleration. *Journal of Geophysical Research*, 91(13), 13423–13431. https://doi.org/10.1029/ja091ia12p13423
- Milan, S. E., Clausen, L. B. N., Coxon, J. C., Carter, J. A., Walach, M.-T., Laundal, K., et al. (2017). Overview of solar wind-magnetosphere-ionosphere-atmosphere coupling and the generation of magnetospheric currents. Space Science Reviews, 206(1–4), 547–573. https://doi.org/10.1007/s11214-017-0333-0
- Øieroset, M., Lin, R. P., Phan, T. D., Larson, D. E., & Bale, S. D. (2002). Evidence for electron acceleration up to 300 keV in the magnetic reconnection diffusion region in the Earth's magnetotail. *Physical Review Letters*, 89(19), 195001. https://doi.org/10.1103/PhysRevLett.89.195001
- Oka, M., Phan, T. D., Krucker, S., Fujimoto, M., & Shinohara, I. (2010). Electron acceleration by multi-island coalescence. *The Astrophysical Journal*, 714(1), 915–926. https://doi.org/10.1088/0004-637X/714/1/915
- Pan, Q., Ashour-Abdalla, M., Walker, R. J., & El-Alaoui, M. (2014). Ion energization and transport associated with magnetic dipolarizations. Geophysical Review Letters, 41(16), 5717–5726. https://doi.org/10.1002/2014GL061209
- Parks, G. K., Arnoldy, R. L., Lezniak, T. W., & Winckler, J. R. (1968). Correlated effects of energetic electrons at the 6.6 Re equator and the auroral zone during magnetospheric substorms. *Radio Science*, 3(7), 715–719. https://doi.org/10.1002/rds196837715
- Pritchett, P. L. (2006). Relativistic electron production during driven magnetic reconnection. Geophysical Research Letters, 33(13), L13104. https://doi.org/10.1029/2005GL025267
- Pritchett, P. L. (2008). Collisionless magnetic reconnection in an asymmetric current sheet. *Journal of Geophysical Research*, 113(A12), A06210. https://doi.org/10.1029/2007JA012930
- Quinn, J. M., & Southwood, D. J. (1982). Observations of parallel ion energization in the equatorial region. *Journal of Geophysical Research*, 87(10), 10536–10540. https://doi.org/10.1029/ia087ia12p10536
- Retinò, A., Nakamura, R., Vaivads, A., Khotyaintsev, Y., Hayakawa, T., Tanaka, K., et al. (2008). Cluster observations of energetic electrons and electromagnetic fields within a reconnecting thin current sheet in the Earth's magnetotail. *Journal of Geophysical Research*, 113(A12), A12215. https://doi.org/10.1029/2008JA013511
- Ricci, P., Lapenta, G., & Brackbill, J. U. (2003). Electron acceleration and heating in collisionless magnetic reconnection. *Physics of Plasmas*, 10(9), 3554–3560. https://doi.org/10.1063/1.1598207
- Richard, L., Khotyaintsev, Y. V., Graham, D. B., Vaivads, A., Nikoukar, R., Cohen, I. J., et al. (2022). Proton and helium ion acceleration at magnetotail plasma jets. *Journal of Geophysical Research: Space Physics*, 127(8), e2022JA030430. https://doi.org/10.1029/2022JA030430
- Runov, A., Grandin, M., Palmroth, M., Battarbee, M., Ganse, U., Hietala, H., et al. (2021). Ion distribution functions in magnetotail reconnection: Global hybrid-Vlasov simulation results. *Annales Geophysicae*, 39(4), 599–612. https://doi.org/10.5194/angeo-39-599-2021
- Shi, F., Lin, Y., Wang, X., Wang, B., & Nishimura, Y. (2021). 3-D global hybrid simulations of magnetospheric response to foreshock processes. Earth, Planets and Space, 73(1), 138. https://doi.org/10.1186/s40623-021-01469-2
- Smets, R., Delcourt, D., Sauvaud, J. A., & Koperski, P. (1999). Electron pitch angle distributions following the dipolarization phase of a substorm: Interball-Tail observations and modeling. *Journal of Geophysical Research*, 104(A7), 14571–14581. https://doi.org/10.1029/1998JA900162
- Thorne, R. M., Bortnik, J., Li, W., & Ma, Q. (2021). Wave-particle interactions in the Earth's magnetosphere. In R. Maggiolo, N. André, H. Hasegawa, D. T. Welling, Y. Zhang, & L. J. Paxton (Eds.), *Magnetospheres in the solar system* (pp. 93–108). https://doi.org/10.1002/9781119815624.ch6
- Torbert, R. B., Russell, C. T., Magnes, W., Ergun, R. E., Lindqvist, P. A., LeContel, O., et al. (2016). The FIELDS instrument suite on MMS: Scientific objectives, measurements, and data products. *Space Science Reviews*, 199(1–4), 105–135. https://doi.org/10.1007/s11214-0109-8
- Ukhorskiy, A. Y., Sitnov, M. I., Merkin, V. G., Gkioulidou, M., & Mitchell, D. G. (2017). Ion acceleration at dipolarization fronts in the inner magnetosphere. *Journal of Geophysical Research: Space Physics*, 122(3), 3040–3054. https://doi.org/10.1002/2016JA023304
- Wang, H., Lu, Q., Huang, C., & Wang, S. (2016). The mechanisms of electron acceleration during multiple X line magnetic reconnection with a guide field. *The Astrophysical Journal*, 821(2), 84. https://doi.org/10.3847/0004-637X/821/2/84
- Wing, S., Gjerloev, J. W., Johnson, J. R., & Hoffman, R. A. (2007). Substorm plasma sheet ion pressure profiles. *Geophysical Research Letters*, 34(16), L16110. https://doi.org/10.1029/2007GL030453
- Yamada, M., Russell, K., & Ji, H. (2007). Progress in understanding magnetic reconnection in laboratory and space astrophysical plasmas. *Physics of Plasmas*, 14(5), 058102. https://doi.org/10.1103/RevModPhys.82.603
- Zelenyi, L. M., Dolgonosov, M. S., Grigorenko, E. E., & Sauvaud, J. (2007). Universal properties of the nonadiabatic acceleration of ions in current sheets. JETP Letters, 85(4), 187–193. https://doi.org/10.1134/S0021364007040017
- Zhou, M., Ashour-Abdalla, M., Deng, X., El-Alaoui, M., Richard, R. L., & Walker, R. J. (2011). Modeling substorm ion injection observed by the THEMIS and LANL spacecraft in the near-Earth magnetotail. *Journal of Geophysical Research*, 116(A8), A08222. https://doi. org/10.1029/2010IA016391
- Zhou, X., Angelopoulos, V., Sergeev, V. A., & Runov, A. (2010). Accelerated ions ahead of earthward propagating dipolarization fronts. *Journal of Geophysical Research*, 115(A5), A00I03. https://doi.org/10.1029/2010JA015481

SHI ET AL. 16 of 16